

## Experimental Test of Two Span Continuous Concrete Beams Reinforced with Hybrid GFRP-Steel Bars

Item Type	Article
Authors	Araba, A.M.;Zinkaah, O.H.;Alhawat, Musab M.;Ashour, Ashraf
Citation	Araba AM, Zinkaah OH, Alhawat M et al (2023) Experimental Test of Two Span Continuous Concrete Beams Reinforced with Hybrid GFRP-Steel Bars. Structures. 47: 2485-2500.
DOI	<a href="https://doi.org/10.1016/j.istruc.2022.12.055">https://doi.org/10.1016/j.istruc.2022.12.055</a>
Rights	© 2023 The Authors. This is an Open Access article distributed under the Creative Commons CC-BY license ( <a href="https://creativecommons.org/licenses/by/4.0/">https://creativecommons.org/licenses/by/4.0/</a> )
Download date	2026-03-05 23:14:27
Link to Item	<a href="http://hdl.handle.net/10454/19210">http://hdl.handle.net/10454/19210</a>

# Experimental Test of Two Span Continuous Concrete Beams Reinforced with Hybrid GFRP-Steel Bars

Almahdi Mohamed Araba<sup>1,2</sup>, Othman Hameed Zinkaah<sup>3</sup>, Musab Alhawat<sup>4\*</sup>, Ashraf Ashour<sup>4</sup>

<sup>1</sup> Arcadis Design & Consultancy, United Kingdom

<sup>2</sup> Civil Engineering Department, University of Wadi Alshatti, Brak, Libya,

<sup>3</sup> Department of Civil Engineering, Al-Muthanna University, Al-Muthanna, Samawah, Iraq

<sup>4</sup> School of Engineering, University of Bradford, UK

\* Corresponding author's e-mail address: [m.m.a.alhawat@bradford.ac.uk](mailto:m.m.a.alhawat@bradford.ac.uk)

## ABSTRACT

The current paper aimed at investigating the flexural performance of five large-scale continuous concrete beams reinforced by both steel bars and glass fibre reinforced polymer (GFRP). All the studied specimens had the same geometrical dimensions, with 200mm width, 300mm depth, and two identical spans of 2600mm. The quantity of longitudinal steel reinforcement, GFRP reinforcement, and hybrid reinforcement ratio at the top and bottom layers of beams were the key parameters explored in this study. The experimental findings indicated that using the hybrid reinforcement of steel and GFRP in multi-span continuous concrete beams exhibited a ductile behaviour. However, the hybrid ratio of steel bars/GFRP is critical for restricting the extent of moment redistribution ratios. Moreover, using the same hybrid reinforcement ratios at sagging and hogging regions led to a limited moment redistribution. On the other hand, the hybrid beams strengthened by various hybrid ratios in the critical sections of the tested beams demonstrated a remarkable moment redistribution up to 43%.

The test results were compared with the available theoretical model and equations for predicting the beams' moment capacity. It was found that the ACI.440.2R-08 reasonably predicted the flexural capacity of tested beams whereas the Yinghao and Yong equation underestimated the flexural capacity in the hogging sections. It was also shown that using the collapse mechanism with plastic hinges at sagging and hogging sections yielded good predictions for the loading capacity of hybrid reinforced concrete continuous beams.

**Keyword:** FRP/steel bars; Continuous beams; Moment redistribution; Ductility, Load capacity prediction

## 1 1 INTRODUCTION

2 Steel reinforced concrete presented excellent structural and economic performance.  
3 Steel reinforcing bars are ductile and have high elastic modulus, however, the  
4 performance of steel reinforced concrete structures is seriously affected by the  
5 exposure to harsh environmental conditions, causing significant corrosion in steel  
6 reinforcement over time. This phenomenon can cause serious consequences on the  
7 structures such as cracking, spalling and losing the bond between steel bars and  
8 concrete, which eventually may lead to losing the serviceability and requiring  
9 fundamental repair works or even demolition [1-3]. The costly maintenance of steel  
10 reinforced concrete structures highlighted the need to find new construction  
11 materials that can offer a better resistance system against the deterioration of  
12 reinforced concrete structures [4]. On the other hand, the use of fibre reinforcement  
13 polymer (FRP) in structures has recently received much worldwide interest owing to  
14 its superior material characteristics such as a superior tensile strength to weight  
15 ratio and its high resistance to corrosion [5, 6]. However, FRP has been criticized  
16 for its relatively brittle behaviour and low elastic modulus [7]. Therefore, the use of  
17 hybrid reinforcement(steel/FRP) in structures seems a promising solution for  
18 enhancing the efficiency of these materials and producing an effective construction  
19 system. This type of reinforcement would be able to provide higher load capacity  
20 over conventional single reinforcement [8-14], in addition to the high possibility of  
21 improving ductility and serviceability. Aiello and Ombres, [8] concluded that the use  
22 of a hybrid combination of AFRP and steel reinforcement in concrete beams would  
23 achieve desirable strength and ductility. In addition, they found that when the  
24 reinforcement ratio exceeded the balanced reinforcement ratio for FRP-reinforced  
25 concrete beams, the contribution of the steel reinforcement to the beams' flexural

1 capacity was less than 15% even if the ratio between the tensile steel reinforcement  
2 and FRP reinforcement is high.

3 In another study, Lau and Pam [9] stated that to prevent excessive elongation that  
4 causes the rupture of FRP reinforcement, the GFRP reinforcement ratio needs to  
5 be higher than that of steel reinforcement as well as the minimum FRP  
6 reinforcement recommended by ACI 440.1R-06. Thus, the hybrid reinforcement  
7 ratio should be selected based on the assumption of occurring steel yield before the  
8 crushing of concrete, whilst the strain in FRP reinforcement needs to be much lower  
9 than FRP rupture strain.

10 Yinghao, L. and Yong, Y. [10] tested the flexural capacity of three Concrete beams  
11 with different arrangements of hybrid GFRP and steel reinforcement. They found  
12 that placing GFRP and steel rebars together at the outer layer is the most effective  
13 way of arranging hybrid reinforcement in terms of ultimate bending moment, but  
14 steel corrosion cannot be easily avoided with this arrangement. The authors also  
15 concluded that a good agreement between deflections experimental results and the  
16 results predicted by Yoon's model, [11]. El-Refai et al. [12] reported that the effective  
17 reinforcement ratio ( $\rho_{eff}$ ) had more influence on the moment-carrying capacity of  
18 the hybrid reinforced beams compared to the axial stiffness ratio; This increase in  
19  $\rho_{eff}$  led to enhancing the moment capacities of the hybrid reinforced beams. A  
20 similar conclusion was reported by Safan [13] and Qu et al. [14].

21 Few investigations were carried out in the literature on single-span beams  
22 strengthened by hybrid FRP and steel bars [8-12], while very limited research was  
23 conducted on continuous supported hybrid reinforced concrete beams [15-17].  
24 During the loading process in statically determined specimens, the bending  
25 moments linearly enhance with increasing the applied load. In continuous beams,

1 however, once the elastic limit of any constituent material is surpassed, the load-  
2 moment connection might become nonlinear. As a result, moment redistribution can  
3 take place, allowing more flexibility in structural design. The redistribution of moment  
4 is mainly controlled by the structural elements' ability to provide sufficient ductility  
5 and providing enough robustness [17,18]. Ductility also enables energy dissipation  
6 during earthquakes, generating substantial deformations, that allow a warning of  
7 impending collapse. However, due to their linear elastic behaviour, FRP bars are  
8 unable to contribute to redistributing internal forces or improving ductility until failure.  
9 Therefore, most design guidelines and standards recommend designing structural  
10 elements that guarantee concrete crushing before the rupture of FRP at ultimate  
11 loading. In addition, moment redistribution is not permitted in multi-span FRP  
12 reinforced continuous concrete structures [19, 20].

13 Araba and Ashour [15] experimentally investigated the flexural behaviour of two-  
14 span continuous concrete specimens reinforced by a combination of steel and  
15 GFRP bars. The findings indicated that sufficient stiffness and ductility can be  
16 achieved after the linear stage, which is mostly determined by the reinforcement  
17 ratio of GFRP/steel. However, the beams exhibited very little or even no moment  
18 redistribution owing to the similarity of hybrid reinforcement in sagging and hogging  
19 zones. Akiel et al. [16] examined twelve two-span concrete slabs, six of them were  
20 reinforced only by Basalt fibre-reinforced polymer (BFRP) bars, while the others  
21 were reinforced with steel and BFRP in both zones (sagging and hogging). They  
22 concluded that the flexural rigidity of critical sections showed little difference in  
23 hybrid-reinforced specimens before the occurrence of steel yielding compared with  
24 their counterparts strengthened only by BFRP bars. On the other hand, the samples

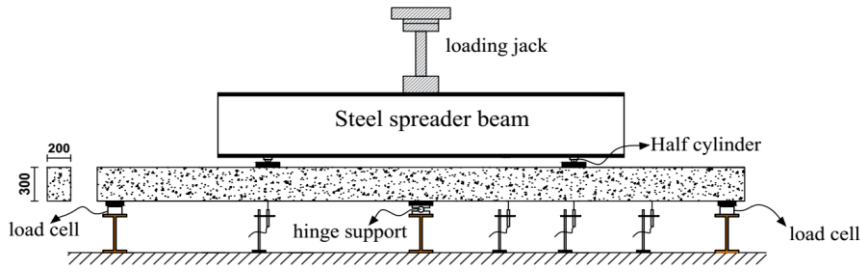
1 reinforced with BFRP bars showed a brittle failure, which occurred by the rupture in  
2 FRP bars.

3 Based on the above-mentioned information, it can be concluded that the use of  
4 hybrid reinforcement (steel/FRP bars) in structural members seems a very effective  
5 solution to enhance the efficiency of construction system by providing higher load  
6 capacity and improving ductility and serviceability. However, very limited research  
7 was found in the literature on the behaviour of large-scale members reinforced with  
8 a hybrid system, especially multi-span continuous beams. Therefore, this research  
9 aims to study the serviceability, moment redistribution and ductility of multi-span  
10 continuous hybrid reinforced concrete beams (steel/GFRP). The applicability of the  
11 available existing equation for predicting the bearing capacity of two-span RC  
12 beams has also been validated with the current findings. The findings obtained from  
13 this study are expected to contribute to developing and establishing guidelines for  
14 designing structural elements reinforced with a hybrid reinforcement system. In  
15 addition, the results may also offer a greater grasp of the nonlinear behaviour of  
16 continuous concrete structures strengthened by GFRP and steel bars to design  
17 practitioners and researchers.

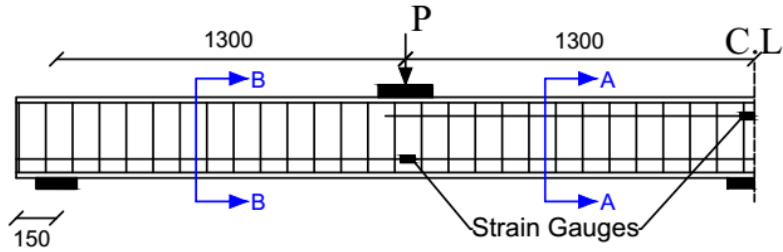
## 18 **2 EXPERIMENTAL PROGRAM**

### 19 **2.1 Specimens Geometrical Dimensions**

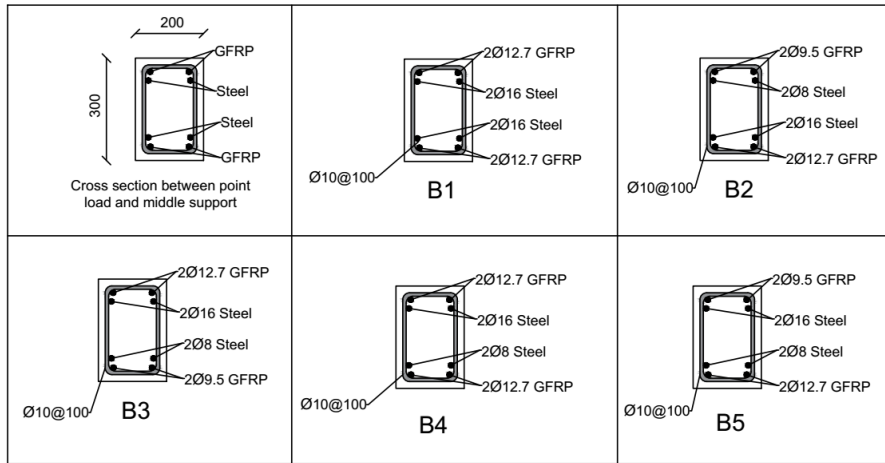
20 The test program consists of five continuous GFRP/ steel reinforced concrete  
21 beams. As depicted in Fig 1, the geometrical dimensions of all specimens were the  
22 same, having 200 mm width, 300 mm depth and two identical spans (2600 mm for  
23 each). The hybrid GFRP/steel reinforcement at sagging and hogging regions was  
24 the main parameter investigated, as explained below.



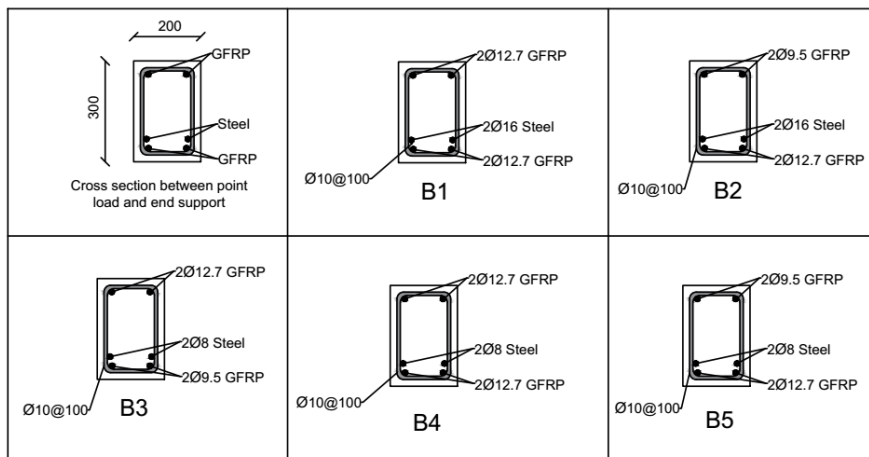
(a) Test setup



(b) Longitudinal view of test specimens and strain gauge locations.



(c) Section A-A



(d) Section B-B

Fig. 1. Geometrical dimensions of the tested specimens.

1

## 2 **2.2 Hybrid Reinforcement Details of Test Specimens**

3 Table 1 and Fig. 1 detail the hybrid reinforcement for all tested specimens. The  
4 specimens were designed based on the sectional analysis of hybrid reinforced  
5 sections as detailed by Kara et al [21]. Fig. 2. plots the boundaries of failure modes  
6 for different GFRP/steel reinforcement combinations. The solid and dotted lines  
7 shown in Fig. 2 demonstrate the boundaries of FRP rupture and concrete crushing  
8 for concrete grades 40 and 70 MPa, respectively. As can be noted from Fig. 2. the  
9 mode of failure between the upper and lower boundary demonstrates the yield of  
10 reinforcing steel prior to the crushing of concrete. The zone of GFRP rupture before  
11 concrete crushing is located beyond the lower boundary, while the concrete  
12 crushing zone before the yield of steel bars is fallen beyond the upper boundary.

13 All sections of hybrid-reinforced, except two sections, were intended to collapse due  
14 to steel yielding followed by concrete crushing, preceding the rapture of GFRP, as  
15 shown in Fig 2. The selection of reinforcement in this study was designed to cover  
16 the influence of different parameters including hybrid reinforcement configurations,  
17 steel reinforcement configurations and GFRP reinforcement configurations in  
18 sagging/hogging zones.

19 The control specimen (beam B1) was reinforced with a similar hybrid reinforcement  
20 ratio in sagging and hogging sections. The beam was reinforced with two  
21 longitudinal steel bars of  $\text{Ø}16$  mm and two GFRP longitudinal bars of  $\text{Ø}12.7$  mm as  
22 represented by point 3 in Fig 2, where concrete crushing is expected to occur before  
23 FRP rupture. Beam B2 was reinforced with the same amount of hybrid  
24 reinforcement used in the bottom side of beam B1 but with a lower reinforcement  
25 ratio on the top side ( $2\text{Ø}8$  mm of steel and  $2\text{Ø}9.5$  mm of GFRP bars), promoting  
26 FRP rupture (point 2). An opposite longitudinal arrangement (GFRP and steel bars)

1 to beam B2 was used for beam B3. In beam B4, the top reinforcement was identical  
2 with that used in beams B3 and B1 (point 3), while the bottom part was strengthened  
3 with 2Ø12.7 mm of GFRP bars and 2Ø8 mm of steel bars (point 1). The top layer of  
4 beam B5 was reinforced by 2Ø9.5mm of GFRP bars and 2Ø16 mm of steel bars  
5 (point 4), whereas the bottom part was made with the same reinforcement used in  
6 B4.

7 The longitudinal FRP and steel reinforcement were located at the first and second  
8 layers providing 30 mm and 80 mm concrete cover respectively. To avoid the  
9 possible occurrence of shear failure, Ø 10 mm steel stirrups were placed at 100 mm  
10 (center to center) along the entire length of all tested beams. It should be mentioned  
11 that the reinforcing steel in the hogging moment region was curtailed beyond the  
12 mid-span point load as shown in Fig 1.

13 Table 1. Reinforcement details and concrete properties for the tested specimens.

Beam notatio n	Reinforcement of mid-span at the bottom (Area mm <sup>2</sup> ) <sup>a</sup>		Reinforcement of over-central support top bars (area mm <sup>2</sup> ) <sup>a</sup>		Reinforcement ratio				Concrete properties (MPa)		
	$A_s$	$A_f^b$	$A_s$	$A_f^b$	$A_s/A_f$		$\rho^c$		$f_{cu}$	$f_{ct}$	$f_r$
					Saggi ng	Hoggin g	Saggi ng	Hoggin g			
B1	2Ø16 (402)	2Ø12.7 (279)	2Ø16 (402)	2Ø12.7 (279)	1.4	1.4	5.30	5.30	50.7	3.1	3.3
B2	2Ø16 (402)	2Ø12.7 (279)	2Ø8 (100.5 )	2Ø9.5 (170)	1.4	0.6	5.30	2.15	69.5	3.6	
B3	2Ø8 (100.5)	2Ø9.5 (170)	2Ø16 (402)	2Ø12.7 (279)	0.6	1.4	2.20	5.30	69.6	3.8	4.2
B4	2Ø8 (100.5)	2Ø12.7 (279)	2Ø16 (402)	2Ø12.7 (279)	0.4	1.4	1.30	5.30	62.2	3.4	
B5	2Ø8 (100.5)	2Ø12.7 (279)	2Ø16 (402)	2Ø9.5 (170)	0.4	2.4	1.30	8.60	66.6	3.5	

<sup>a</sup> Reinforcement details presented are based on section (a-a) shown in Fig.1

<sup>b</sup> Based on the measured reinforcing bar size in Table 2.

<sup>c</sup> Axial stiffness ratio  $\rho = A_s E_s / A_f E_f$ .

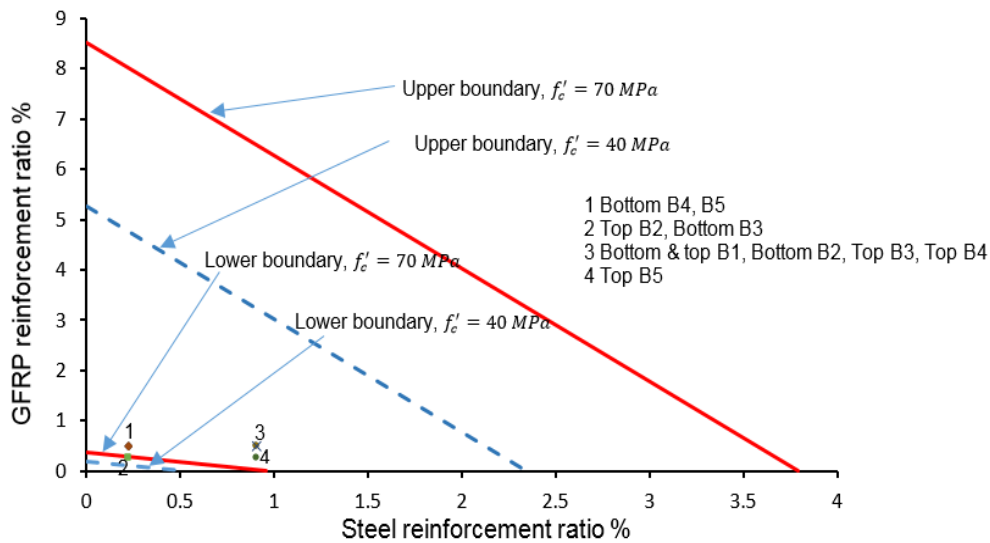


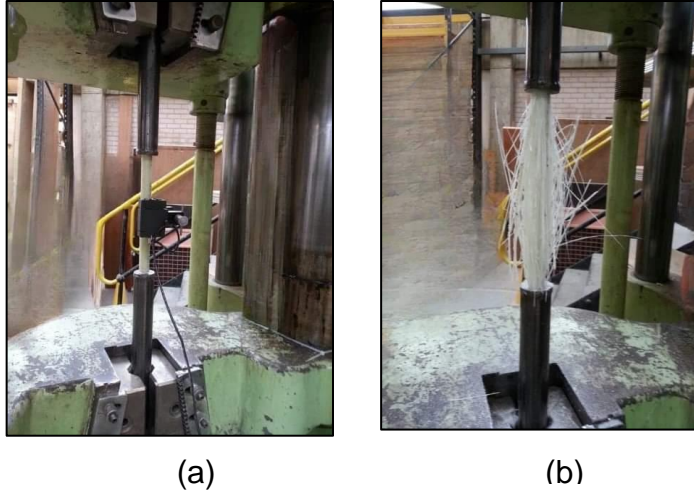
Fig. 2. Flexural failure modes for different GFRP and steel reinforcement combinations.

### 2.3 Material properties

Table 2 shows the characteristics of GFRP and steel reinforcement utilised in the study. The GFRP bars properties were experimentally measured using pull-out tensile test [22], whereas the characteristics of deformed steel were in accordance with the ASTM A615 (2016) [23]. Figure 3 presents one of the tests conducted to measure the tensile test of GFRP bars.

All beams were constructed using ready-mixed concrete which had a 20 mm maximum particle size of aggregate. After casting, all beams were covered by polyethene sheets until the day of testing to prevent losing the moisture needed for the hydration process. On the day of testing each specimen, three cylinders (150 x 300 mm) and three 100 mm cubes were also tested and the mean values of splitting tensile strength ( $f_{ct}$ ) and cube compressive strength ( $f_{cu}$ ) were calculated and presented in Table 1. In addition, the rupture modulus ( $f_r$ ) was acquired from testing two 100x100x500 mm prisms as listed in Table 1. The elasticity modulus of concrete and poisson's ratio were taken as  $4700\sqrt{f'_c}$  and 0.2, respectively. It should

1 be mentioned that, unlike other beams, beam B1 was cast separately with lower  
 2 concrete compressive strengths. Figure 4 shows the construction stages of test  
 3 specimens.



9 Figure 3. Tensile test of GFRP bar (a) during the bar testing, (b) after failure.

10  
11 Table 2. Characteristics of steel and GFRP reinforcements utilised in the  
12 specimens

Bar type	Bar diameter (mm)	Modulus of elasticity (GPa)	Tensile strength (MPa)	Yield strength (MPa)	Rupture strain	Yield strain
Longitudinal Steel	8	200	N/A	580	-	0.0029
	16	200	N/A	580	-	0.0029
Longitudinal GFRP	9.50 (10.40*)	55	1100	N/A	0.020	N/A
	12.70 (13.33*)	55	1200	N/A	0.021	N/A
Steel stirrups	10	200	N/A	580	-	0.0029

\* Bar diameter measured according to ACI 440.3R-12 [22]

13

1  
2  
3  
4  
5  
6  
7  
8  
9  
10  
11  
12  
13  
14  
15  
16  
17  
18  
19  
20  
21  
22  
23  
24  
25  
26  
27  
28  
29  
30  
31  
32  
33  
34  
35

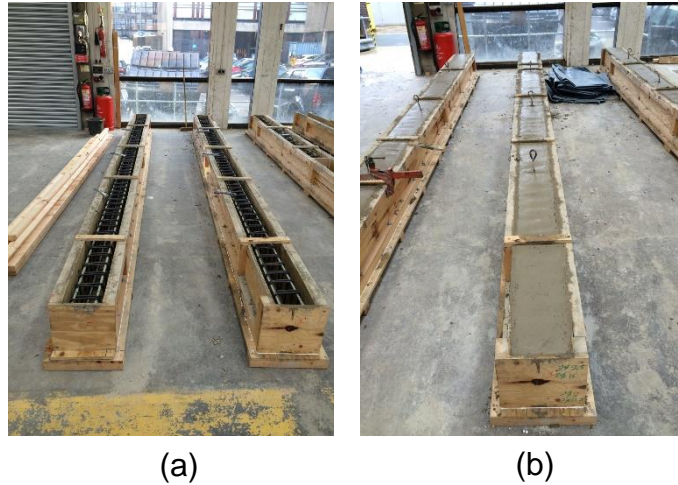
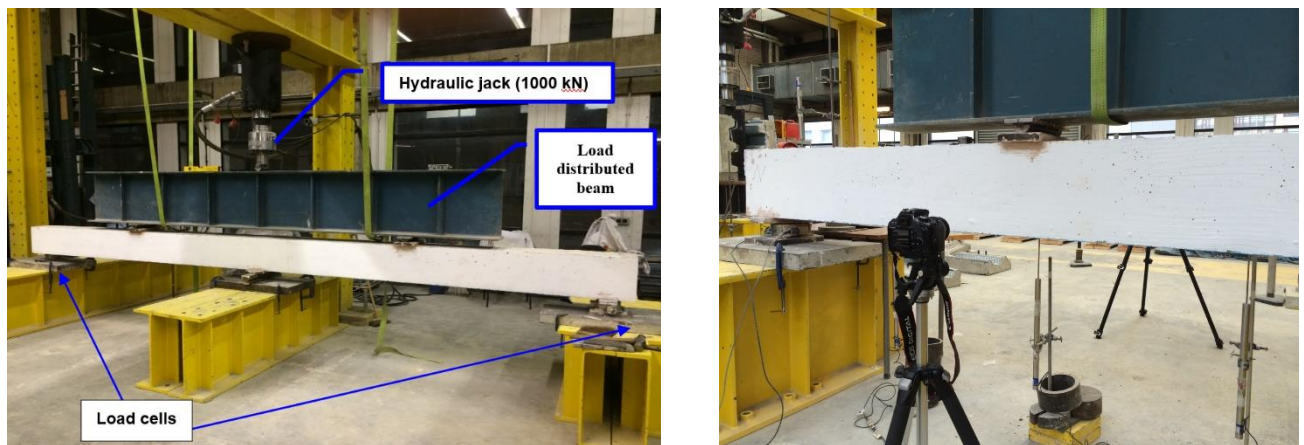


Fig. 4. Construction stages of test specimens, (a) formwork preparations, (b) concrete after casting.

### 2.4 Test rig and instrumentation

The tested beams had two identical spans supported by one central hinge support and two end rollers as shown in Fig. 5. As illustrated in Fig 1, the specimens were loaded at each span using an independent steel reaction frame and a hydraulic ram. The applied load and two end supports reactions were determined via three load cells. Moreover, seven linear variable differential transducers (LVDTs) were connected with the specimens to record the deflections at different locations. Three LVDTs were installed to measure any movement at the middle and two end supports. The vertical deflections at the two mid-spans of each specimen were recorded using two LVDTs. The last two LVDTs were utilised to equally record the deflections on one span of the beams at a spacing of  $L/4$ , where  $L$  represents the specimen span length. The variation of reinforcing steel strain during loading, at sagging and hogging regions, was recorded using three electrical resistance strain (ERS) gauges had 5 mm length, whilst a data logger was utilised to automatically record the readings obtained from load cells, strain gauges and LVDTs at the applied load.



(a)

(b)

Figure 5. (a) Test setup, (b) Some devices used in the experiments.

### 3. RESULTS AND DISCUSSIONS

#### 3.1 Crack propagation and reinforcement strains

Figure 6 demonstrates the patterns of crack occurred in continuous hybrid reinforced concrete beams at failure, whereas Table 3 illustrates the visible cracking load of all tested beams at mid-span and over the central support. The first visible crack was observed in the hogging region. From Fig. 6, it can easily be noted that cracks are more located around the middle support in the hogging zone of beam B3, in comparison with beam B2, whereas the opposite results were observed in the sagging regions of these beams. In terms of beam B4, the first crack was simultaneously reported at a load of 35 kN at mid-span and over middle support.

As the same hybrid reinforcement ratio was used in beams B4 and B5 at mid-span sections, a very similar cracking pattern was observed in the vicinity of the mid-span region. By comparing beams B5 with B2, it can be noted that the effect of increasing the reinforcing steel ratio at the total applied load of 240 kN has become more pronounced and led to the formation of a larger number of cracks in the hogging

1 zone. This might be attributed to the high axial stiffness of steel reinforcement,  
 2 governing the crack widths, where smaller crack spacings were formed.

3

4

5

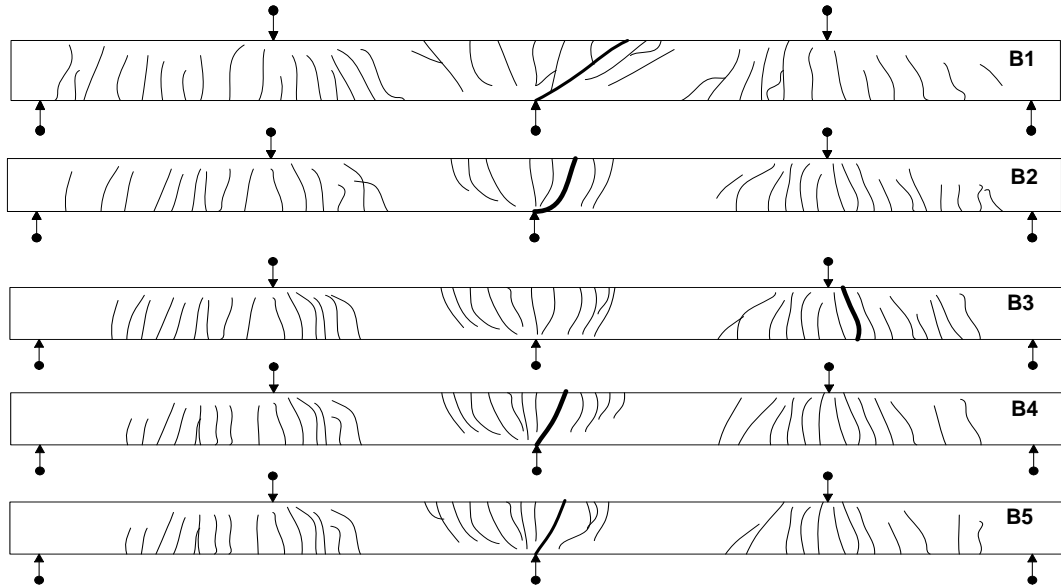
6

7

8

9

10



11

Fig. 6. Failure cracking patterns of the specimens tested.

12

13

14

15

Table 3. First cracking, yield and failure loads of the tested specimens.

Beam notation	$P_{cr}$ (kN)		$P_y$ (kN)		$P_u$ (kN)	Observed failure mode
	Sagging	Hogging	Sagging	Hogging		
B1	43	40	310	255	465	Flexure-tension failure at middle support and mid-span.
B2	45	40	288	145	452	GFRP rupture over middle support.
B3	40	35	155	238	364	GFRP rupture at mid span.
B4	35	35	175	210	450	Flexure-tension failure at middle support and mid-span.
B5	30	25	180	165	423	Flexure-tension failure at middle support and mid-span.

where  $P_{cr}$  is first cracking,  $P_y$  is the yield load and  $P_u$  is the ultimate load.

Note:  $P_{cr}$ ,  $P_y$  and  $P_u$  are the total loads applied on each specimen tested.

16

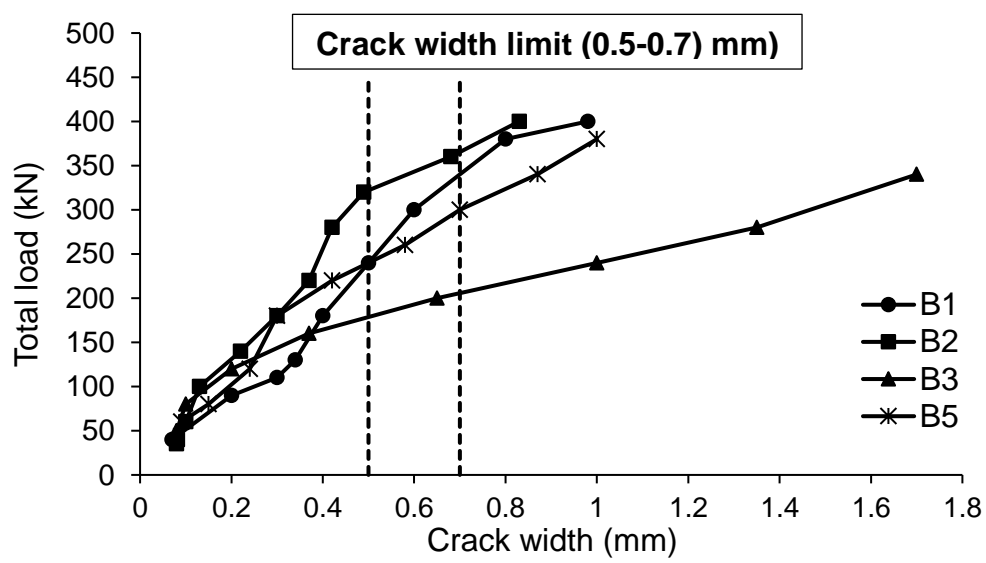
17 Fig. 7 presents the relationship between the total applied load and cracking width at

18 the mid-span. The cracking widths were measured using two high-quality digital

19 cameras. The images captured were subsequently processed using version 6.0 of

1 Image-Pro Plus software. The serviceability limits of cracking width specified by  
 2 CAN/CSA S6-06 [24] (0.5 mm for elements exposed to exterior exposure and 0.7  
 3 mm for other elements) were also included in Fig 7 for comparison purposes at the  
 4 service load of 67% of ultimate loads in Table 3. The crack width results of B4 were  
 5 not addressed in Fig 7 because of malfunctioned cameras.

6 It was also observed that flexural crack widths are highly dependent on the hybrid  
 7 reinforcement ratio. In comparison with beam B1, beam B2, which was strengthened  
 8 at mid-span by the same reinforcement ratio, exhibited fewer widths of cracks at the  
 9 same level of loading. This reduction in crack widths might be ascribed to the higher  
 10 compressive strength of concrete of B2. The cracking width in beam B2 was less  
 11 than 0.5 mm, which corresponded to the service load, while beam B3 recorded a  
 12 crack width higher than 0.7 mm at the service load, highlighting the influence of the  
 13 mid-span reinforcement ratio. According to beams B1 and B5, it is noted that the  
 14 requirements for interior exposure were only obtained, while the exterior criteria  
 15 were not met.

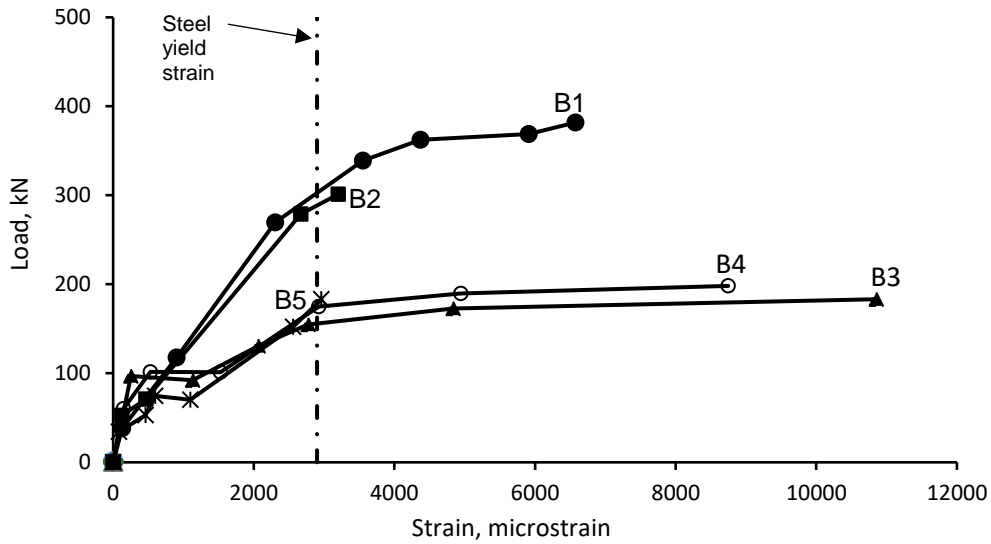


16

17

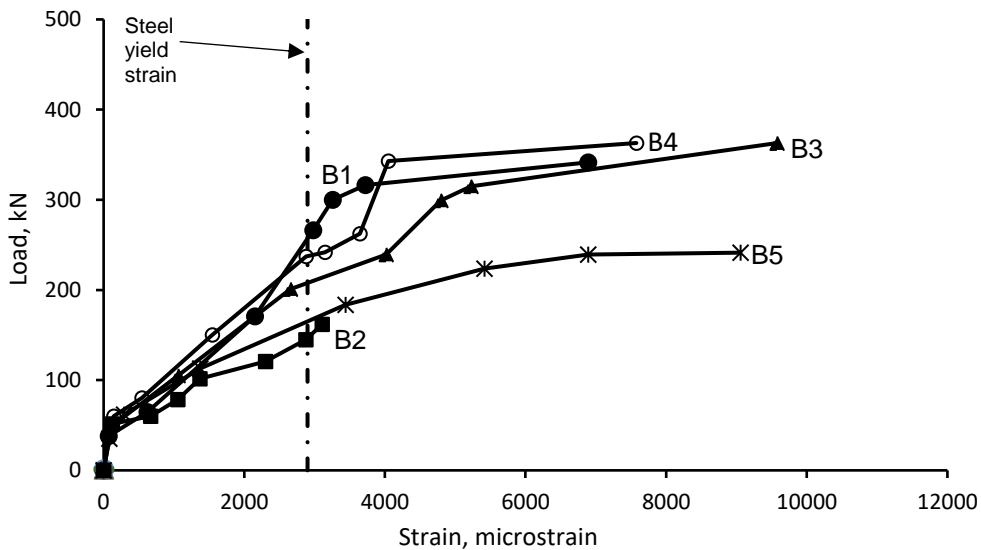
Fig. 7. Crack width at the mid-span of the tested specimens.

1 Figs. 8 and 9 show the tensile strain behaviour of reinforcing steel during loading.  
2 Fig. 8, presents the tensile steel strain in the sagging section against the total  
3 applied loading, while Fig. 9 shows the tensile steel strain at the internal support  
4 against the total applied loading. Generally, the test specimens exhibited a tri-linear  
5 steel strain response. Prior to reaching the cracking stage, the tensile strains of the  
6 longitudinal steel bars were extremely low, whilst a sudden increase in the strain of  
7 the tensile steel reinforcement was noticed in the sagging/hogging zones after the  
8 formation of cracks. For specimen B2, the steel yielded first in the hogging region.  
9 Conversely, the tensile steel reinforcement in the sagging zone yielded first in beam  
10 B3. This is mainly attributed to the appropriate hybrid reinforcement ratio used,  
11 especially the number of steel bars at the middle support and mid-span sections in  
12 beams B3 and B2, respectively, where less reinforcement was found at middle  
13 support and mid-span sections of these beams, respectively. Moreover, the tensile  
14 steel bars, in beams B4 and B5 in the sagging zones, yielded almost at the same  
15 loading level, reflecting the similarity of the bottom hybrid reinforcement ratio. In  
16 specimens B2 and B5, the experimental tensile steel strain response in the hogging  
17 and sagging zones, respectively, was not fully captured beyond a certain load as  
18 shown in Figs. 8 and 9 as a result of strain gauge malfunction.



1  
2  
3  
4  
5  
6

Fig. 8. Total applied load against tensile steel strains at the mid-span of the tested beams.



7  
8  
9  
10  
11

Fig. 9. Total applied load against tensile steel strains at middle support of the tested beams.

### 3.2 Failure modes

12  
13  
14  
15  
16  
17

During the current work, different failure modes were observed, corresponding to the variations in the behaviour of the tested beams. Three specimens, B1, B4 and B5 failed in a ductile manner as a result of reinforcing steel yielding in the tension zone, followed by crushing in concrete at sagging and hogging zones (See Fig 10).

1 The failure in B2 and B3, on the other hand, occurred due to GFRP rupture over the  
2 middle support and mid-span areas, respectively, (See Figs 10-B and 10-C).

3 As shown in Fig 10-A, a ductile failure was stated in beam B1 due to the yielding of  
4 tensile steel bars prior the crushing of concrete. In the continuous hybrid beam B2,  
5 GFRP bars ruptured in the hogging region before the crushing of concrete in the  
6 compressive zone, followed by yielding in tensile steel reinforcement in the sagging  
7 region as presented in Fig 10-B. On the other hand, beam B3 exhibited an opposite  
8 failure to that of B2 as illustrated in Fig 10-C. Beam B3 showed sagging flexural  
9 failure owing to steel reinforcement yielding in the tension zone of the mid-span  
10 region earlier than that at the central support, where the rupture of GFRP bars took  
11 place. In addition, the over support and mid-span sections of specimens B2 and B3,  
12 respectively, experienced wide cracks, indicating the occurrence of GFRP bars  
13 rupture, as predicted in Fig 2 and depicted in Figs 10-B and 10-C.

14 The failure of specimen B2 was mainly due to GFRP bars rupture in the hogging  
15 moment area before the crushing of concrete in the sagging moment area.  
16 Conversely, the crushing of concrete was observed in beam B3 at the mid-span  
17 after the rupture of GFRP over intermediate support. For hybrid beams B4 and B5,  
18 the failure was initiated due to the crushing of concrete in the middle support section,  
19 followed by concrete crushing in the sagging moment zone, and wide cracking at  
20 the middle support section.

21

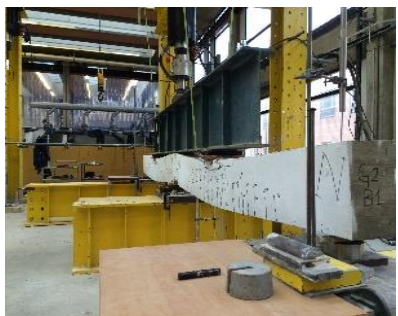
22

23

24

1

Deformed shape near failure



Failure at Middle support region



Failure at Mid-span region

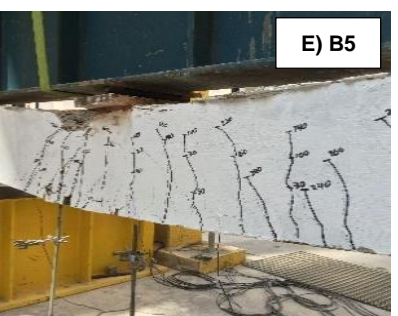
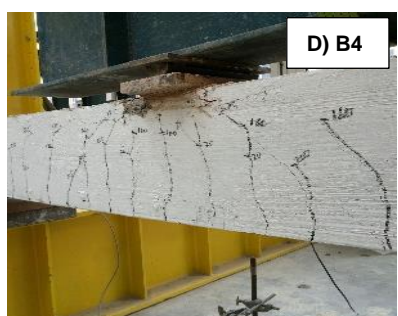
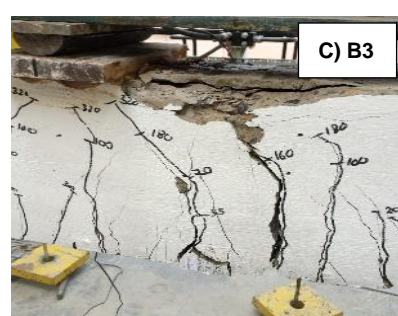
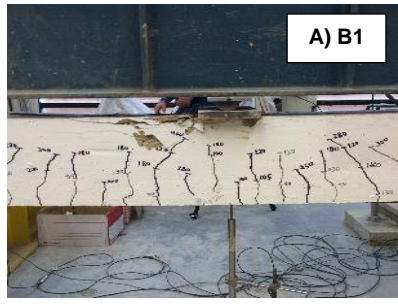


Fig. 10. Failure modes of tested beams.

### 1 **3.3 Load Deflection Response**

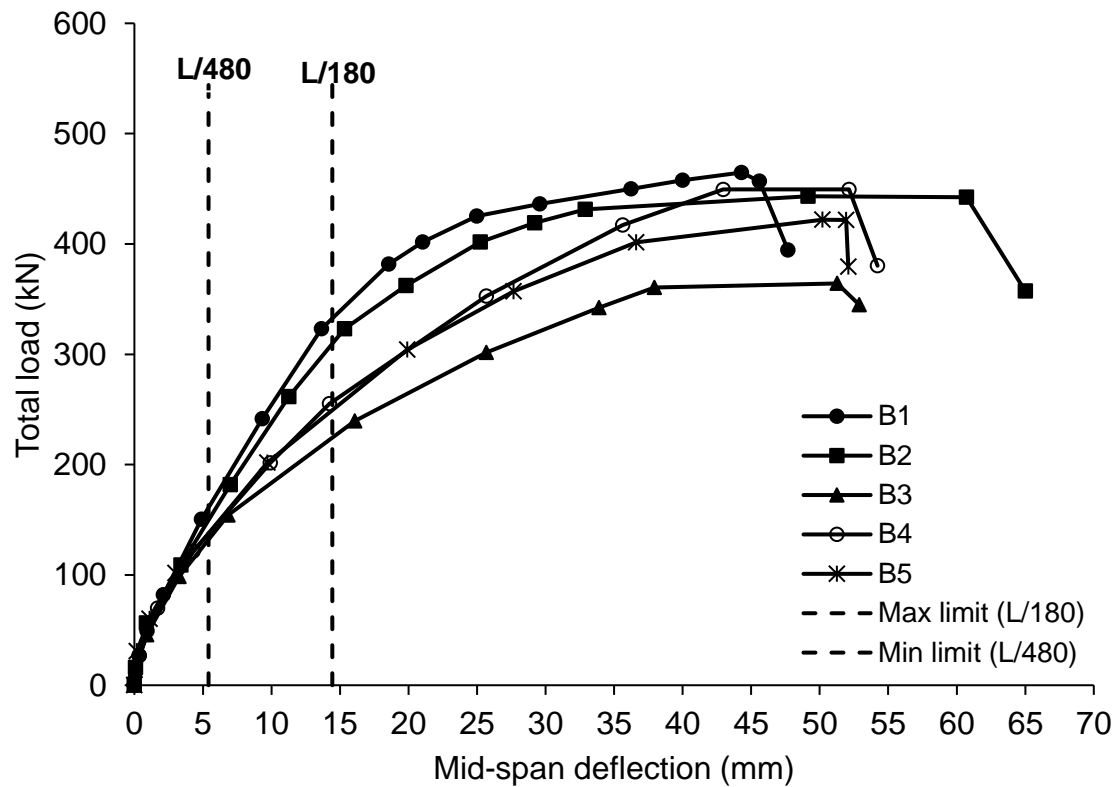
2 The relationship between the total applied load and the mid-span deflections of  
3 specimens is depicted in Fig. 11. All specimens illustrated linear load-deflection  
4 behaviour up to the cracking load. After cracking, the results showed that the flexural  
5 rigidity of the mid-span section had an impact on the stiffness reduction in the tested  
6 specimens, as shown in Fig. 11. Generally, the ratio of hybrid steel-GFRP  
7 reinforcement at the mid-span section is one of the main factors for reducing the  
8 deflections of the tested beams. This behaviour can be explained by the predicted  
9 enhancement of the flexural stiffness at mid-span. It can also be observed that beam  
10 B3 showed higher deflection compared to B2 at the same level of loading, since the  
11 flexural stiffness of B2 was greater than what was recorded in the sagging moment  
12 zone in B3.

13 Regarding the effect of the area of GFRP bars at the hogging section on load-  
14 deflection response, Fig. 11 shows that beam B4 was slightly stiffer than beam B5  
15 beyond a load value of approximately 350 *kN*. This was observed although the  
16 sagging zone in beams B4 and B5 were reinforced with the same hybrid  
17 reinforcement ratio. This mostly resulted from the differences in the top area of  
18 GFRP bars at the hogging zone. On the other hand, the influence of GFRP  
19 reinforcement ratio in the sagging area on load-deflection behaviour could be easily  
20 observed by comparing specimens B3 with B4. Both beams were reinforced by the  
21 same ratio of steel and hybrid reinforcement at hogging and sagging sections,  
22 respectively. In comparison with beam B3, B4 provided higher flexural stiffness at  
23 failure loading, while approximately the half of deflection value was recorded.

24 The allowable deflection is mainly controlled by the function and type of the structure  
25 element. The Canadian Standard Association CSA S806-12 [20] recommends the

1 allowable deflection to be between  $L/480$  -  $L/180$  (5.5mm -15 mm, where L is the  
 2 beam span). It was found that the deflection value corresponding to the calculated  
 3 service load (67% of ultimate load) for the hybrid beams (B1, B2, B3, B4 and B5)  
 4 was 5, 20, 16, 20 and 18 mm, respectively. It should be noted that the deflections  
 5 associated with the service loading did not achieve the serviceability limit of the  
 6 investigated beams. The results obtained could be utilised to establish a guideline  
 7 to provide a suitable hybrid reinforcement ratio, and thus, the achieved stiffness  
 8 behaviour of beams strengthened by hybrid reinforcement might be fallen within the  
 9 serviceability limits.

10



11  
12

Fig. 11. Load-deflection response of the tested beams.

13

### 3.4 Redistribution of Support Reactions

14

15 Because the beams were statically indeterminate, the end support responses were  
 16 assessed using two load cells. Therefore, the actual internal forces (i.e., bending  
 17

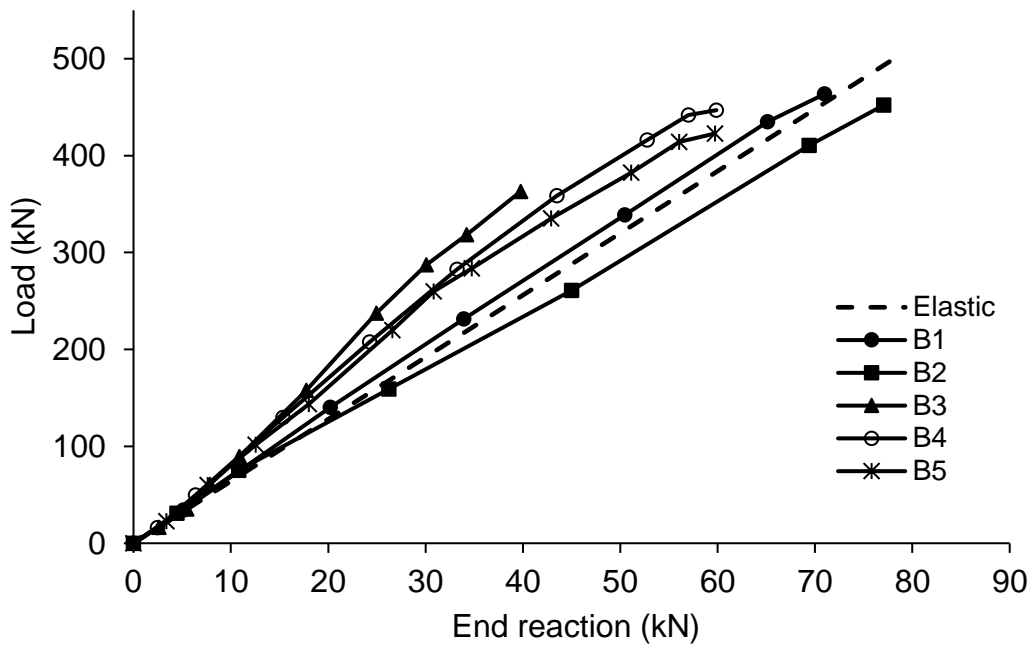
1 moments) were obtained by measuring the end support reactions( $R$ ) along the  
2 length of the specimens.

3 Figs. 12 and 13 show the end support reaction and middle support reaction against  
4 the total applied loading for the tested specimens, respectively. As the two end  
5 support reactions were quite similar because of the symmetrical arrangement, only  
6 one end support reaction was presented in Fig 12. To compare the measured  
7 reactions with the calculated ones, the calculated end support reaction ( $R=0.3125P$ )  
8 and middle support reaction ( $R=1.375P$ ) taken from the elastic analysis were also  
9 plotted in Figs. 12 and 13, respectively. As expected, the measured end support  
10 reactions of all tested beams were almost identical with the calculated ones before  
11 the crushing of concrete due to the linear elastic characteristic of concrete as shown  
12 in Fig 12.

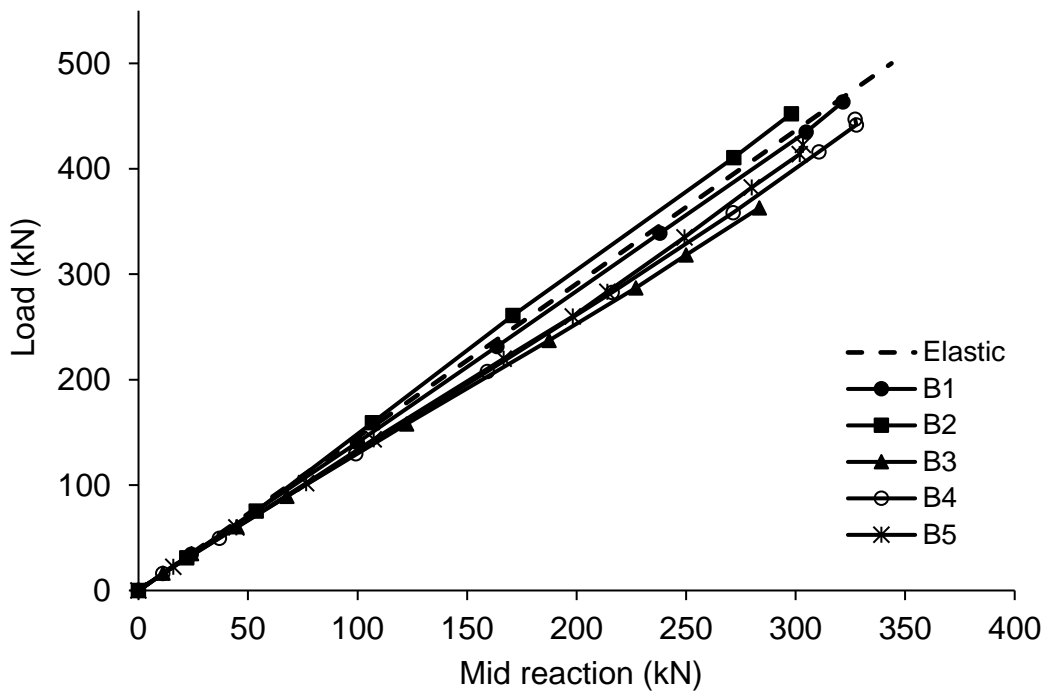
13 The hybrid beams demonstrated a remarkable load redistribution after cracking,  
14 except for specimen B1, indicating signs of moment redistributions between the  
15 sagging and hogging zones. The end support reaction of B1 remained close to that  
16 obtained from the elastic analysis, since a similar reinforcement was provided in  
17 sagging and hogging areas. The results also showed that the reaction of the end  
18 support for beam B2 was slightly high compared to the elastic one, indicating the  
19 redistribution of load from the mid-support to the mid-span as a result of the higher  
20 axial stiffness in the mid-span region.

21 On the contrary, beam B3 showed an opposite reaction response to beam B2,  
22 because of the reverse reinforcement arrangement of beam B3 in comparison with  
23 beam B2. Beams B4 and B5 demonstrated similar load redistribution behaviour up  
24 to reaching about  $150\text{ kN}$ , and then beam B4 exhibited larger moment redistribution  
25 until failure. This increase in moment distribution might be explained by the higher

1 GFRP reinforcement ratio in the hogging section in beam B4 compared with beam  
 2 B5.



3  
 4 Fig. 12. Load-end support reactions of the tested specimens.  
 5



6  
 7 Fig. 13. Load-Middle support reactions of the tested specimens.  
 8  
 9  
 10  
 11

### 1 **3.5 Bending Moments Redistribution**

2

3 To evaluate the moment redistribution ratio ( $\beta$ ) in the tested beams, the measured

4 bending moments in sagging and hogging zones and the elastic bending moment

5 diagrams along the hybrid continuous beam span at failure were plotted in Fig 14.

6 The moment redistribution ratio ( $\beta$ ) at the mid-span and over support sections could

7 be obtained by comparing the measured values with the elastic bending moments

8 as given by Eq. (1):

$$9 \quad \beta = \left( \frac{M_m - M_e}{M_e} \right) \times 100\% \quad (1)$$

10 where  $M_m$  is the experimental bending moment taken from the measured load and

11  $M_e$  is the moment calculated from the elastic analysis. The positive value of  $\beta$  at a

12 certain section represents the increase of moment at the calculated section due to

13 redistribution from another section at failure, whereas the negative value indicates

14 the opposite behaviour.

15 Regardless of B1, Fig. 14 shows that the distribution of the measured moment at

16 failure is significantly different from that elastically calculated. The similar distribution

17 of elastic and experimental bending moment distribution of B1 is mainly because of

18 using the same top and bottom reinforcement arrangements along the beam length,

19 leading to obtaining similar stiffness at the middle support and mid-span zones. The

20 increased reinforcement ratio at the hogging zone also lowered the rotational

21 capability at the middle support. The moment redistribution from sagging to hogging

22 regions occurred in hybrid beams B1, B3, B4, and B5 as shown in Figs 14-A, 14-C,

23 14-D and 14-E, respectively, On the other hand, the redistribution of moments from

24 the hogging to sagging zone occurred only in hybrid beam B2 as seen in Fig 14-B,

25 which might be explained by the sufficient moment capacity in the region. The

26 results also showed that the area and steel reinforcement arrangement had a

1 profound influence on the moment redistribution ratio at failure. The smaller area of  
2 hybrid reinforcement in the sagging region of continuous beams, the higher moment  
3 redistribution ratio, as shown in Fig 14-C (beam B3). However, it is important to  
4 mention that increasing the area of GFRP reinforcement in the bottom side, resulted  
5 in decreasing the moment redistribution ratio, which can be noticed by comparing  
6 hybrid beams B3 and B4. Moreover, the increase of GFRP area in the hogging  
7 section did not show any effect on moment redistribution as observed from beams  
8 B4 and B5. Generally, the larger amount of reinforcement in the middle support  
9 section contributes to controlling the crack widths, which resulted in making hogging  
10 areas stiffer than mid-span sections. Hence, the moment redistribution from the  
11 sagging to the hogging moment zone is taken place.

12 By comparing the measured bending moments with the elastic ones at failure for  
13 each specimen, it could be observed that beam B2 redistributed up to 15% of the  
14 hogging bending moment (See Fig. 14-B), whereas beams B3, B4 and B5  
15 redistributed up to 43%, 19% and 18% of sagging bending moments as shown in  
16 Figs 14-C to 14-E, respectively.

17

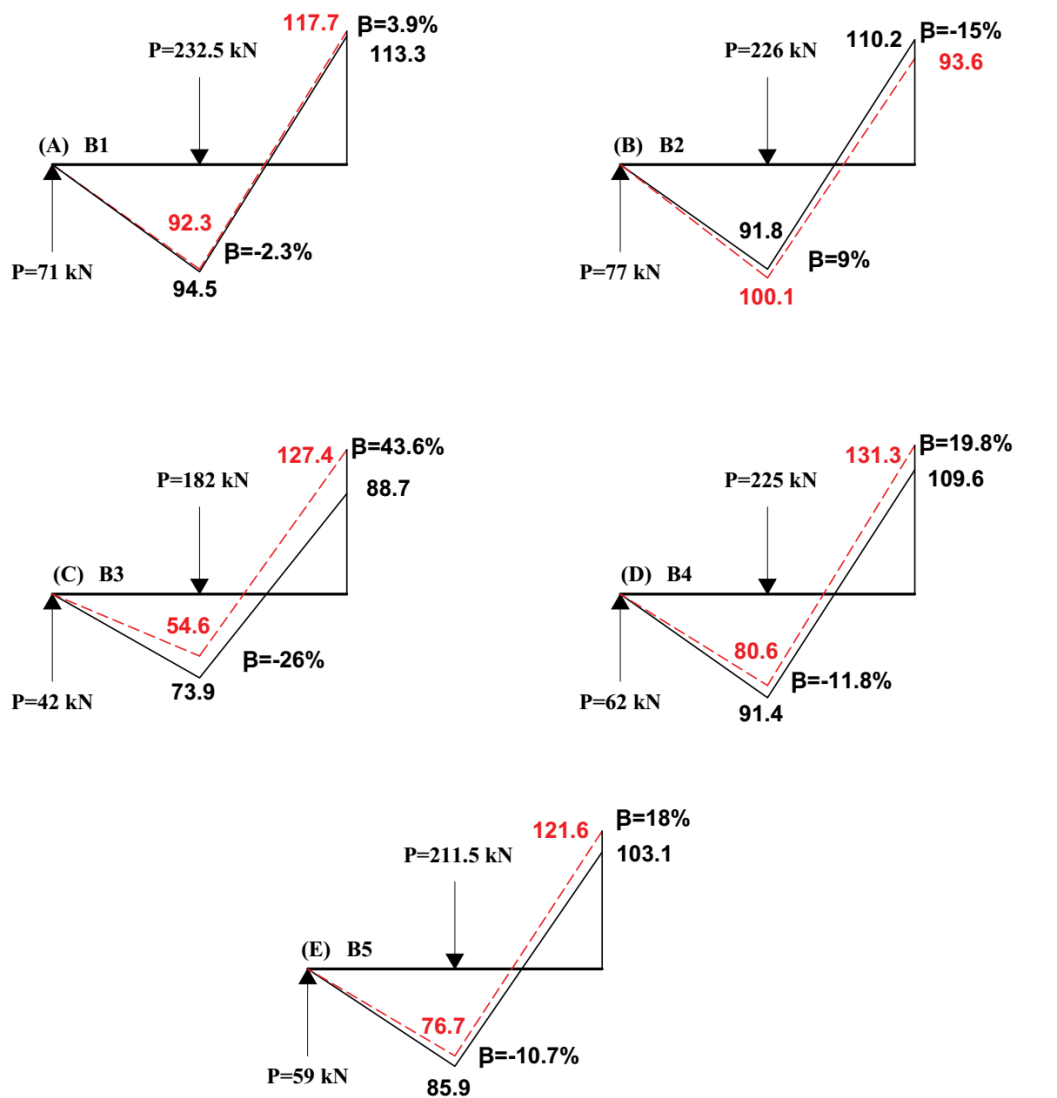
18

19

20

21

22



- 1
  - 2
  - 3
- - - Measured bending moment (kN.m)       $P$  Load at failure (kN)  
— Elastic bending moment (kN.m)       $R$  End reaction at failure (kN)

4 Fig 14. Measured versus elastic bending moment diagrams at failure.

5

6 The current standards permit a ratio of moment redistribution at the ultimate load for

7 RC continuous beams, based on the strain level at the internal steel reinforcement.

8 However, the divergence from the elastic response is also controlled by crack

9 development, and hence a considerable percentage of moment redistributions may

10 occur at low load values. Based on this assumption, the analysis of moment

11 redistributions for the tested beams during loading appears pertinent as described

1 in Fig. 15. For specimens B1, B4 and B5a, a positive redistribution of moments was  
2 always noted in the hogging region, whilst there was a negative moment  
3 redistribution at the sagging zone over the whole inelastic range. Beams B2 and B3  
4 exhibited different behaviour from others. For B2, the moment redistribution was  
5 reported negative at the mid-span, and positive at the middle support before  
6 vanishing and gradually exhibits an opposite behaviour with the continued applied  
7 load. Beam B3 demonstrated an inverse behaviour to B2, as shown in Fig. 15.  
8 However, the anomalous behaviour of B3 during the very early stage could be  
9 attributed to the occurrence of premature cracking at the mid-span, accompanied  
10 by initial redistribution toward the inner support.

11 The first cracking load in the hogging region, as presented in Table 3, was between  
12 12.5 to 20kN (note the load shown in Fig. 15 is the mid-span point load which is  
13 one-half of the loads presented in Table 3). Therefore, the beginning of moment  
14 redistribution took place with the formation of the first crack in each tested beam.

15 The moment redistribution ratio increased after steel yielding except for B1. The  
16 steel bars in B1, B2 and B5 initially yielded in the hogging zone at a load of 127.5  
17 kN, 72.5 kN and 82.5 kN, respectively (one-half of the loads presented in Figs 8 and  
18 9). On the other hand, steel bars in B3 and B4 first yielded in the sagging region at  
19 a load of 77.5 kN and 87.5 kN, respectively (one-half of the loads presented in Figs  
20 8 and 9).

21 By comparing the results shown in Fig. 14 at failure with the results presented in  
22 Fig. 15 over the entire inelastic range, it can be seen that all specimens exhibited  
23 higher moment redistributions before failure. The maximum moment redistribution  
24 ratios before failure in the hogging zone of beams B1, B2, B3, B4 and B5 were 13%,  
25 17%, 55%, 42% and 40%, respectively. Beam B5 which was strengthened by less

1 reinforcement of steel bars in the mid-span showed a higher moment redistribution  
2 ratio than beam B2. However, B3 showed the highest moment redistribution ratio,  
3 which was strengthened by low GFRP reinforcement in the sagging region and  
4 higher GFRP reinforcement in the hogging section compared with beam B5. The  
5 comparison between the results obtained from beams B3 and B4 showed more  
6 influence of the GFRP reinforcement ratio in the sagging section, whereas by  
7 comparing beams B4 and B5, the results presented higher impact of GFRP bars in  
8 the hogging section. When the reinforcement of GFRP bars in the sagging section  
9 is higher than that of the hogging section, the opposite arrangement is expected in  
10 the section. Thus, the section would develop a higher ratio of moment redistribution  
11 as shown in B2 and B5.

12 Therefore, to achieve high moment redistribution ratios, the hybrid reinforcement  
13 ratio in one critical section should be smaller than that of other critical sections.  
14 However, the small amount of hybrid reinforcement should be positioned in the  
15 hogging section to guarantee the moment redistribution is out of the hogging region  
16 as illustrated in beam B2.

17 As can be seen in Figs. 14 and 15, the experimental findings demonstrated that the  
18 amount of redistribution is mainly dependent on two stages, namely crack  
19 development, which contributes to about 40-55 % of the total redistribution, and  
20 steel yielding. In addition, of course, the reinforcement configuration is considered  
21 the key parameter for controlling the amount of moment redistribution ratio.

22

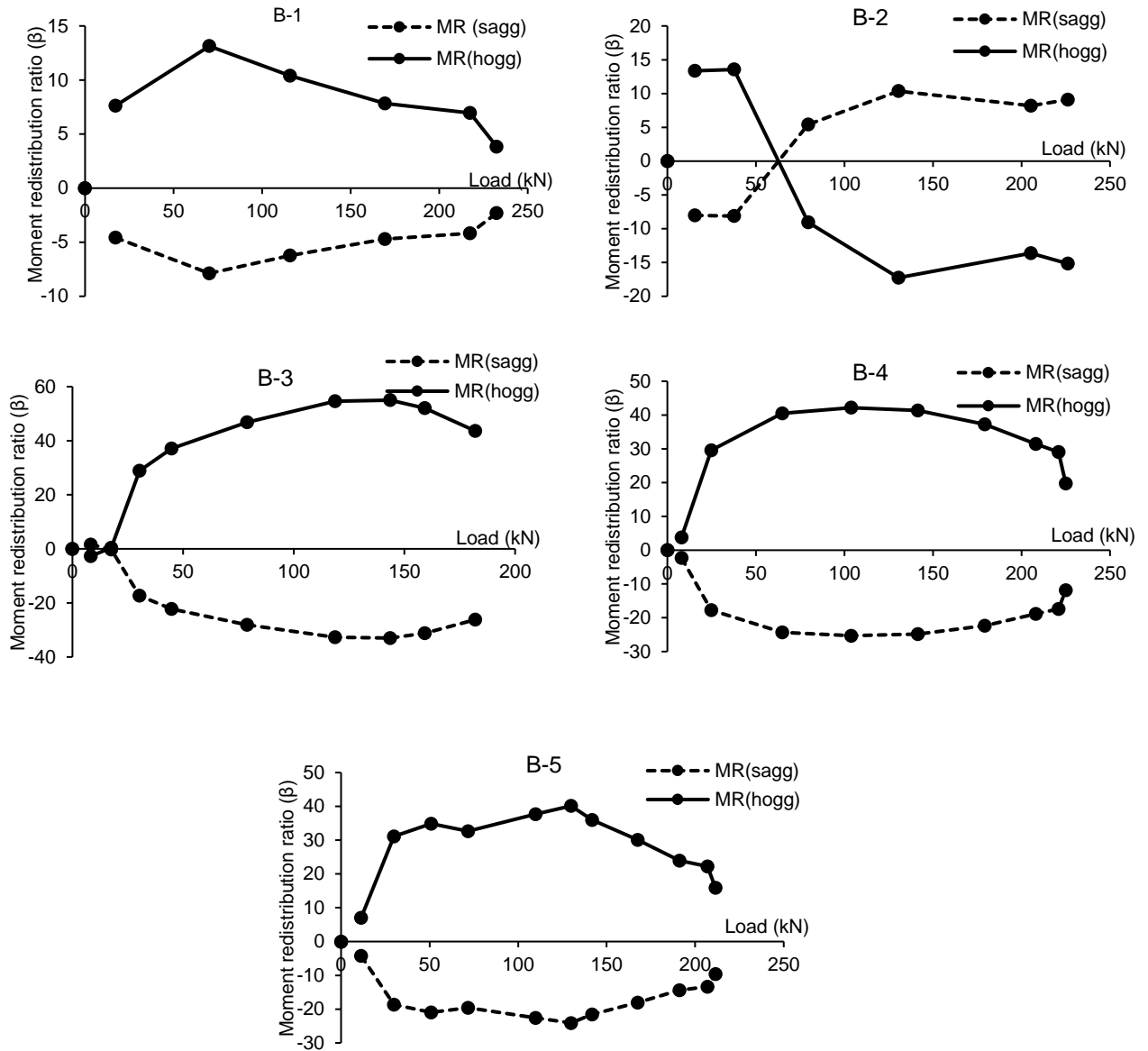


Fig. 15. Total variation of  $\beta$  with applied load for the tested specimens.

1  
2  
3  
4  
5  
6  
7  
8  
9  
10

11 The values of the moment redistribution factor ( $\beta$ ) at both the mid-span (sagging  
12 moment) and over the middle support (hogging moment) for the tested beams are  
13 summarised in Table 4. For all hybrid continuous beams, the value of  $\beta$  at the  
14 hogging section was found always to be greater than the ones at the sagging  
15 section, and the ratio of hogging to sagging moment redistribution ( $\lambda$ ) is  
16 approximately 1.67 for all tested beams. This study confirmed the results of [21] that

1 the redistribution of moment at the hogging zone is about 60% higher than the  
 2 sagging moment redistribution, as calculated in Table 4.

3  
 4  
 5

Table 4. Moment redistribution at failure of tested beams.

Beam notation	Moment redistribution, $\beta$ %		$\lambda^a$
	Sagging	Hogging	
B1	-2.3	3.7	-1.60
B2	9.0	-15.0	-1.67
B3	-26.0	43.6	-1.67
B4	-11.8	19.8	-1.67
B5	-10.7	18.0	-1.68

<sup>a</sup>  $\lambda$  = ratio of hogging to sagging moment redistribution.

6  
 7  
 8

#### 4. Beam Ductility

9 The ductility in beams can be described as the ability of beams to withstand inelastic  
 10 deformation without losing its load-carrying capacity before reaching failure. For  
 11 traditional RC elements, the ductility can be computed as the ratio of deformation,  
 12 expressed as curvature, rotation or displacement [25], at ultimate load to that at the  
 13 first yield of reinforcing steel. This is mostly due to the fact that steel exhibits obvious  
 14 higher plastic deformation once it is being yielded. However, since the beams tested  
 15 in this investigation were strengthened by hybrid steel/FRP reinforcement and FR,  
 16 deformation and energy-based approaches were employed to evaluate the flexural  
 17 ductility of the tested beams.

18  
 19  
 20

##### 4.1 Deformation Based Method

21 The deflection ductility index,  $\mu_{\Delta 1}$ , was selected to assess the ductility index of the  
 22 tested specimens by using Eq. 5 [25].

23 
$$\mu_{\Delta} = \frac{\Delta_u}{\Delta_y} \quad (5)$$

1 where  $\Delta_u$  and  $\Delta_y$  are the mid-span deflections corresponding to the ultimate load  
 2 and tensile steel yielding load in either the tension side of mid-span section or over  
 3 support regions (the second shift in the slope of the load-deflection response).

#### 4 **4.2 Energy Based Method**

5  
 6 It has been reported [26] that the ductility of structural members can be determined  
 7 from the ratio between the total energy and the elastic energy at failure loading as  
 8 described in Fig 16. The ductility index ( $\mu_{en}$ ) based on the energy method was given  
 9 by Eq. 6 [26].

$$10 \quad \mu_{en} = 0.5 \left( \frac{E_{tot}}{E_{ela}} + 1 \right) \quad (6)$$

11 where  $E_{tot}$  ( $= E_{inel} + E_{ela}$ ) is the total energy, represents the region located under the  
 12 loading deflection curve up to the failure, and  $E_{ela}$  is the recovered elastic energy in  
 13 the case of unloading as illustrated in Figs 16 and 17.  $E_{ela}$  can be determined from  
 14 the unloading test. However, if such result is not obtained, the elastic energy can be  
 15 computed from the triangle area created between the failure load and the slope of  
 16 the two initial straight lines of the load deflection curve, as illustrated in Fig 16. The  
 17 failure load might be described as either the ultimate load (as taken in this study) or  
 18 that corresponding to 80% of the ultimate load. The calculated  $E_{ela}$  and  $E_{inel}$  and  
 19  $\Delta_{el}$  from experimental results are presented in Table 5.

20 Table 5: Calculated energy and experimental values of deflection

21	Beam no	$E_{ela}$ (kN.mm)	$E_{inel}$ (kN.mm)	$\Delta_{el}$ (mm)
22	B1	3349	11348	16.2
23	B2	3133	16298	15.9
24	B3	3525	16847	13.1
	B4	5430	17562	17.2
	B5	4314	14845	17.1

25 The experimental deflection ( $\mu_{\Delta}$ ) and energy ductility ( $\mu_{en}$ ) for each beam are shown  
 26 in Table 6. To obtain the ductility index  $\mu_{\Delta}$ , the deflections at the lower yielding load

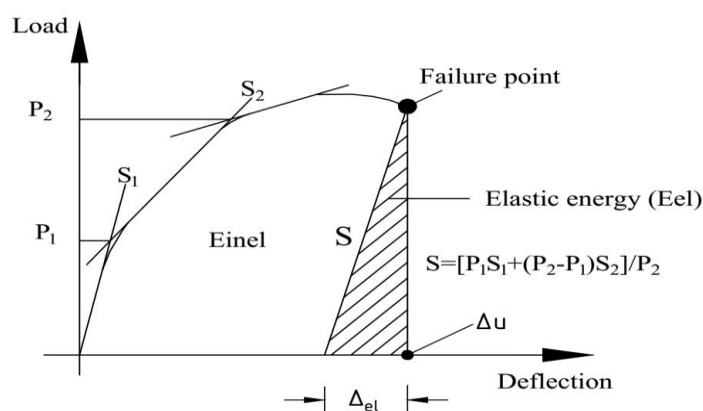
1 of the tensile reinforcement in the sagging or hogging zones was utilised as shown  
 2 in Table 6. The ratios of energy ductility to displacement ductility are also presented  
 3 in Table 5. The comparison showed that the ratios of energy ductility to  
 4 displacement ductility ranged between 40-60% for all examined specimens.  
 5 As shown in Table 6, hybrid beam B2 exhibited a higher energy ductility index than  
 6 that of specimens B1, B3, B4 and B5 due to the earlier yielding of the flexural  
 7 reinforcement at the hogging zone in B2. Moreover, Fig 17 shows the ultimate load  
 8 of beam B2 stayed almost constant with an extended displacement range (long  
 9 plateau). On the other hand, the other beams exhibited a shorter plateau, and the  
 10 residual capacity and the corresponding displacement were still considerable as  
 11 shown in Fig 17.

12

Table 6. Experimental values of deflections and ductility ratios of the test beams.

Beam no	$\Delta_y$ (mm)	$\Delta_u$ (mm)	$\mu_\Delta$	$\mu_{en}$	$\frac{\mu_{en}}{\mu_\Delta}$
B1	10	45	4.5	2.70	0.6
B2	6	60	10	3.60	0.36
B3	7	51	7.29	3.40	0.47
B4	9	52	5.8	2.62	0.45
B5	8	52	6.50	2.72	0.42

13  
14



15  
16  
17  
18  
19  
20

Fig. 16. Total, elastic, and inelastic energies (Naaman and Jeong, [26]).

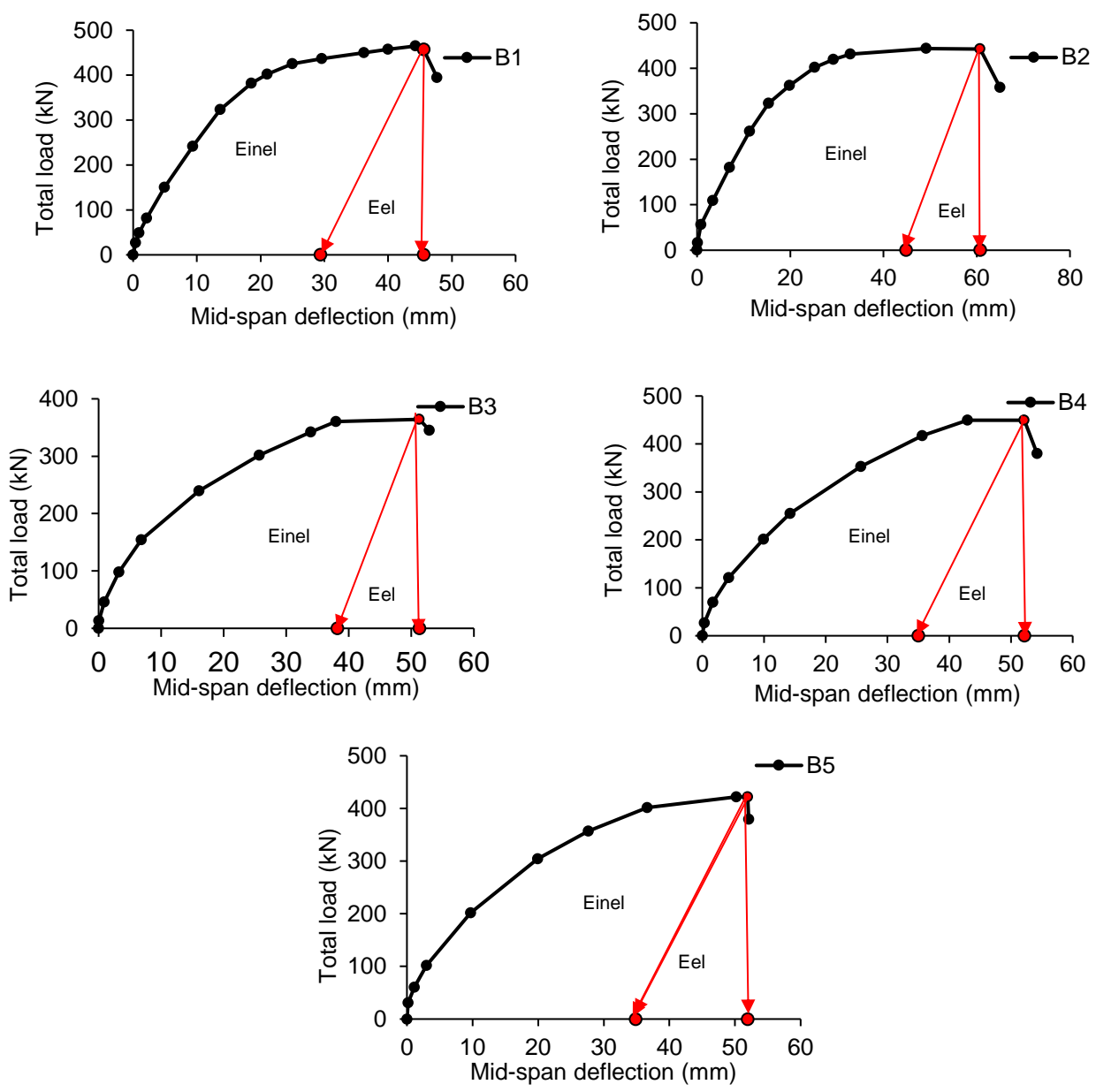


Fig. 17. Total applied load versus mid span deflection of the tested specimens.

### 5. Flexural Load Capacity Prediction

The calculations of the flexural strength of the tested beams considered the equilibrium condition and assumed that the sections of middle support and mid-span reached their flexural capacities of  $M_{uh}$  and  $M_{us}$ , respectively. As presented in ACI 440.2R.08 [27], the equilibrium of stresses and strain compatibility are both considered in calculating the load capacity. Therefore, the applied load ( $P_u$ ) at the

1 mid-span is determined from Eq 7. It should be noted that the self-weight of the  
2 specimen is not considered.

$$3 \quad P_u = \frac{2}{L}(M_{uh} + 2M_{us}) \quad (7)$$

4 where  $M_{uh}$  is the moment capacities of mid-span (sagging),  $M_{us}$  is the moment  
5 capacities over central support (hogging), and  $L$  represents the length of the span.

6 The reason behind choosing the ACI 440.2R.08 is that the strengthening of RC  
7 structure is one type of hybrid construction in which FRP reinforcement is placed  
8 close to the exterior surface area.

9 Additionally, the two methods developed by Pang et al [28] and Yinghao and Yong  
10 [8] were utilised to estimate the flexural behaviour of hybrid sections. The predicted  
11 moments of resistance and the experimental moments for both middle support and  
12 mid-span sections at failure are described in Table 7. The results showed good  
13 agreement between the calculated and measured values, with accuracy ratios  
14 ranging from 0.99 to 1.34 as shown in Table 8.

Table 7. Comparison between the predicted and experimental moment capacities of the tested beams.

Beam notation	Experimental moment at failure, $M_{exp}$ (kN.m)		Predicted moment at failure, $M_{pre}$ (kN.m)								$\frac{M_{exp}}{M_{pre}}$		Yinghao and Yong (2013) [8]	
			ACI 440.2R.08 [26]		Pang et al, (2015) [27]		Yinghao and Yong (2013) [8]		ACI 440.2R.08 [26]					
	Sagging	Hogging	Sagging	Hogging	Sagging	Hogging	Sagging	Hogging	Sagging	Hogging	Sagging	Hogging	Sagging	Hogging
B1	92.3	117.7	88.00	117.0	99.8	99.8	78.4	78.4	1.05	1.01	0.92	1.18	1.18	1.50
B2	100.1	93.6	99	100	109	64.5	84.8	55	1.01	0.94	0.92	1.45	1.18	1.70
B3	54.6	127.4	62	107	64.5	109	54.8	85	0.88	1.19	0.85	1.17	1.00	1.50
B4	75.8	131.3	79	93	74	105	67.4	83	0.96	1.41	1.02	1.25	1.12	1.58
B5	76.7	121.6	81	92	76	95	68.4	73	0.95	1.32	1.01	1.28	1.12	1.67
Average									0.97	1.17	0.94	1.27	1.12	1.59
Standard deviation									6%	20%	7%	11%	7%	9%

Table 8. Comparison between the predicted and experimental failure loads of the tested beams.

Beam notation	Experimental Failure load, $P_{exp}$ (kN)	Predicted failure load, $P_{pre}$ (kN)					$\frac{P_{exp}}{P_{pre}}$	
		ACI 440.2R.08 [26]		Pang et al, (2015) [27]		Yinghao and Yong (2013) [8]		
		ACI 440.2R.08 [26]	Pang et al, (2015) [27]	Yinghao and Yong (2013) [8]	ACI 440.2R.08 [26]	Pang et al, (2015) [27]	Yinghao and Yong (2013)	
B1	465	451	461	362	1.03	1.01	1.29	
B2	452	458	435	346	0.99	1.04	1.31	
B3	364	355	366	299	1.02	0.99	1.22	
B4	450	386	389	335	1.17	1.16	1.34	
B5	423	391	380	323	1.08	1.11	1.31	
Average					1.06	1.06	1.29	
Standard deviation					7%	7%	5%	

$P_{fd}$  is the predicted failure load based on fully ductile materials

## 6. Conclusions

The current study investigated the flexural performance of five specimens made of two-span continuous concrete beams strengthened by hybrid steel/GFRP reinforcement bars were reported. Based on the findings obtained from the experimental work, the following conclusions can be drawn:

- The beams reinforced with varying hybrid reinforcement ratios in the sagging and hogging zones exhibited more ductile behaviour than those reinforced with similar hybrid reinforcement ratios in both regions.
- Adding more steel or GFRP reinforcement resulted in improving the flexural stiffness of hybrid beams after the first cracking. However, the stiffness of continuous concrete beams is more reliant on the hybrid reinforcement in the sagging region than that found in the hogging region.
- Similar hybrid reinforcement ratios in sagging/hogging areas led to limited moment redistribution behaviour. On the other hand, hybrid beams strengthened by varying hybrid reinforcement ratios in critical sections demonstrated a remarkable moment redistribution up to 43% at failure.
- The stiffness of critical sections is a key factor in determining the direction of moment redistribution whether from mid-span to middle support or vice versa.
- The energy-based methods seem to be more appropriate for predicting the ductility index of concrete beams reinforced by hybrid GFRP/steel beams than deformation methods because a result of their is difficult to predict the steel yield point by the deformation approaches.

- Using the collapse mechanism with plastic hinges at sagging/ hogging zones yielded good predictions for the load capacity of hybrid reinforced concrete continuous beams.
- Based on the data collected from other studies and the findings obtained from the current study, it is suggested for the future work to conduct further investigations on the parameters that control the behaviour of hybrid reinforced beams, such as compressive strength, the area of FRP/steel reinforcement and different types of FRP bars. Furthermore, it is also recommended to investigate the behaviour of FRP/steel reinforced concrete beams made from eco-friendly sustainable materials. Geopolymer concrete might be the right choice as it can be produced with zero Portland cement content [29, 30].

## References

- [1] Zinkaah, O. H., Ashour, A. and Sheehan, T. Experimental tests of two-span continuous concrete deep beams reinforced with GFRP bars and strut-and-tie method evaluation. *Composite Structures*, 2019. 216(112-126).
- [2] Alhawat, M. and Ashour, A., 2019, June. Bond strength between corroded steel reinforcement and recycled aggregate concrete. *Structures*, 19, 369-385.
- [3] Zinkaah, O. H. and Ashour, A. Load capacity predictions of continuous concrete deep beams reinforced with GFRP bars. *Structures*, 2019.19:449-462.
- [4] Zinkaah, O. H., Sultan, H. K., Al-Rifaie, A., and Alridha, Z. (2022). Influence of strut geometry on the size effect of FRP reinforced simply supported deep beams: A theoretical analysis. *Mathematical Modelling of Engineering Problems*, 9(2), 411-417. doi:10.18280/mmep.090215.
- [5] E, Zavvar. Hosseini, A.S. Lotfollahi-Yaghin, M.A. Stress Concentration Factors in Steel Tubular KT-Connections with FRP-Wrapping under Bending Moments. *Structures (Elsevier)*, Volume 33, October 2021, Pages 4743-4765. <https://doi.org/10.1016/j.istruc.2021.06.100>
- [6] Sadat Hosseini, E. Zavvar, and H. Ahmadi, "Stress concentration factors in FRP-strengthened steel tubular KT-joints," *Appl. Ocean Res.*, vol. 108, no. December 2020, p. 102525, 2021, <https://doi.org/10.1016/j.apor.2021.102525>
- [7] Alhawat, M. and Ashour, A., 2020. Bond strength between corroded steel and recycled aggregate concrete incorporating nano silica. *Construction and Building Materials*, 237, 117441.
- [8] Aiello, M. A. and Ombres, L. 2002. Structural performances of concrete beams with hybrid (fiber-reinforced polymer-steel) reinforcements. *ASCE Journal of Composites for Construction*, 6 (2), 133-140.
- [9] Lau, D. and Pam, H. J. 2010. Experimental study of hybrid FRP reinforced concrete beams. *Engineering Structures*, 32(12), 3857-3865.
- [10] Yinghao, L. and Yong, Y. 2013. Arrangement of hybrid rebars on flexural behavior of HSC beams. *Composites Part B: Engineering*, 45(1), 22-31.
- [11] Yoon, Y. S., Yang, J. M., Min, K. H. and Shin, H. O. Flexural strength and deflection characteristics of high-strength concrete beams with hybrid FRP and steel bar reinforcement. 10th International Symposium on Fiber-Reinforced Polymer Reinforcement for Concrete Structures 2011, FRPRCS-10, in conjunction with the ACI Spring 2011 Convention, 2011.
- [12] EL Refai, A., Abed, F. and AL-Rahmani, A. 2015. Structural performance and serviceability of concrete beams reinforced with hybrid (GFRP and steel) bars. *Construction and Building Materials*, 96, 518-529.

- [13] Safan, M. A. 2013. Flexural Behavior and Design of Steel-GFRP Reinforced Concrete Beams. *ACI Materials Journal*, 110(6). 677-686.
- [14] Qu, W., Zhang, X. and Huang, H. 2009. Flexural behavior of concrete beams reinforced with hybrid (GFRP and steel) bars. *ASCE Journal of Composites for construction*, 13 (5), 350-359.
- [15] Araba, A.M. and Ashour, A.F., 2018. Flexural performance of hybrid GFRP-Steel reinforced concrete continuous beams. *Composites Part B: Engineering*, 154, pp.321-336.
- [16] Akiel, M.S., El-Maaddawy, T. and El Refai, A., 2018. Serviceability and moment redistribution of continuous concrete members reinforced with hybrid steel-BFRP bars. *Construction and Building Materials*, 175, pp.672-681.
- [17] Beeby, A.W., 1997. Ductility in reinforced concrete: why is it needed and how is it achieved? *Structural Engineer*, 75(18).
- [18] Li, L., Zheng, W. and Wang, Y., 2019. Review of moment redistribution in statically indeterminate RC members. *Engineering Structures*, 196, p.109306.
- [19] ACI Committee 440, 2015, Guide for the Design and Construction of Concrete Reinforced with FRP Bars, (ACI 440.1R-15), Farmington Hills, Mich. USA American Concrete Institute.
- [20] Canadian Standards Association (CSA). 2012. "Design and construction of building components with fibre-reinforced polymers." CSA Standard S806-12, Rexdale, Ont., Canada.
- [21] Kara, I.F., Ashour, A.F. and Koroğlu, M.A., 2015. Flexural behavior of hybrid FRP/steel reinforced concrete beams. *Composite Structures*, 129, pp.111-121.
- [22] ACI Committee 440, 2012. "Guide test methods for fiber reinforced polymers FRPs for reinforcing or strengthening concrete structures." *ACI 440.3R-14*, Farmington Hills, Mich.
- [23] ASTM Standard A615/A615M, Standard Specification for Deformed and Plain Carbon-Steel Bars for Concrete Reinforcement. 2016.
- [24] Canadian Standards Association S6-06 (2006). Canadian Highway Bridge design code. Canadian Standards Association, Mississauga, Ontario, Canada.
- [25] ZOU, P. X. 2003. Flexural behavior and deformability of fiber reinforced polymer prestressed concrete beams. *ASCE Journal of composites for Construction*, 7(4), 275-284.
- [26] Naaman, A. and Jeong, S. 1995, 'Structural Ductility of Concrete Beams Prestressed with FRP Tendons,' *Non-Metallic (FRP) Reinforcement for*

Concrete Structures, Proceedings of the Second International RILEM Symposium (FRPRCS-2), E & FN Spon, London.

[27] ACI Committee 440, 2008, Guide for the design and construction of externally bonded FRP systems for strengthening concrete structures. (ACI 440.2R-08), Farmington Hills, Mich. USA American Concrete Institute.

[28] Pang, L., Qu, W., Zhu, P. and Xu, J. 2015. Design propositions for hybrid FRP-steel reinforced concrete beams. *ASCE Journal of Composites for Construction*, 20 (4), 04015086.

[29] Zinkaah, O. H., Alridha, Z., and Alhawat, M. (2022). Numerical and theoretical analysis of FRP reinforced geopolymer concrete beams. *Case Studies in Construction Materials*, 16, e01052.

[30] Zinkaah, O. H., Al-Rifaie, A., and Alhawat, M. M. (2021, October). Predictability of existing standard codes for the flexural strength of beams produced from alkali-activated concrete. In *AIP Conference Proceedings* (Vol. 2404, No. 1, p. 080031). AIP Publishing LLC.